Published in final edited form as:
Acta Biomater. 2012 April ; 8(4): 1530–1542. doi:10.1016/j.actbio.2011.12.015.

Aligned Silk-Based 3D Architectures for Contact Guidance in Tissue Engineering

A.L. Oliveira[1,2,3,4], **L. Sun**[3], **H. J. Kim**[3], **X. Hu**[3], **W. Rice**[3], **J. Kluge**[3], **R. L. Reis**[1,2], and **D. L. Kaplan**[3]

[1]3B's Research Group - Biomaterials, Biodegradables and Biomimetics, University of Minho, Headquarters of the European Institute of Excellence on Tissue Engineering and Regenerative Medicine, AvePark, 4806-909 Taipas, Guimarães, Portugal

[2]ICVS/3B's - PT Government Associate Laboratory, Braga/Guimarães, Portugal

[3]Department of Biomedical Engineering, Tufts University, Medford, Massachusetts 02155, USA

[4]Department of Health Sciences, Portuguese Catholic University, Viseu, Portugal

Abstract

An important challenge in the biomaterials field is to mimic the structure of functional tissues via cell and extracellular matrix (ECM) alignment and anisotropy. Toward this goal, silk-based scaffolds resembling bone lamellar structure were developed using a freeze-drying technique. The structure could be controlled directly by solute concentration and freezing parameters, resulting in lamellar scaffolds with regular morphology. Different post-treatments were investigated to induce water stability, such as methanol, water annealing and steam sterilization. The resulting structures exhibited significant differences in terms of morphological integrity, structure and mechanical properties. the lamellar thicknesses were around ~2,6 μm for the methanol treated scaffolds and ~5,8 μm for water-annealed. These values are in the range of the reported for human lamellar bone. Human bone marrow-derived mesenchymal stem cells (hMSCs) were seeded on these silk fibroin lamellar scaffolds and grown under osteogenic conditions to assess the effect of the microstructure on cell behaviour. Collagen in the newly deposited ECM, was found aligned along the lamellar architectures. In the case of methanol treated lamellar structures the hMSCs were able to migrate into the interior of the scaffolds producing a multilamellar hybrid construct. The present morphology constitutes a useful pattern onto which hMSCs cells attach and proliferate for guided formation of a highly oriented extracellular matrix.

Keywords

Silk fibroin; scaffold; freeze-drying; directional freezing; tissue engineering; lamellar morphology; cell alignment

*Corresponding author: Ana L. Oliveira, 3B's Research Group - Biomaterials, Biodegradables and Biomimetics, University of Minho, Headquarters of the European Institute of Excellence on Tissue Engineering and Regenerative Medicine, AvePark, 4806-909 Taipas, Guimarães, Portugal, Ph: +351-253-510908; Fax: +351-253-510909. analeite@dep.uminho.pt, david.Kaplan@tufts.edu.

1. Introduction

The potential of silk as a biomaterial has been widely recognized due to its processing versatility, impressive mechanical performance, biocompatibility, oxygen and water vapor permeability and tailorable degradability [1–3]. Silk-fibroin (SF) is a structural protein that can be extracted from larvae cocoons of the species *Bombyx mori*. In the process of preparing new SF-based biomaterials, microstructure, porosity and surface chemistry are important features that modulate cell behavior, migration and proliferation, towards the desired engineered tissue [4]. Based on this knowledge, SF has been generated in a wide variety of morphologies for engineering different tissues in terms of structure and function [5–13].

Most functional tissues such as musculoskeletal, tendon and ligament, cardiac, nervous, and vascular present significant cell alignment and anisotropic morphologies. To mimic such intricate structures and develop materials with properties/functions direction-controlled constitutes an important challenge and has drawn considerable interest in recent years. A significant amount of research has been directed towards controlling the spatial organization of cells in well-defined microarchitectures [14–18]. Several techniques have been described to control two-dimensional cellular alignment [15, 17, 19]. However, cellular organization within 3D architectures remains challenging. Considerable progress has been achieved using strategies of mechanical [20, 21], electrical [22] or magnetic [23] stimulation. Still, there is a need for simple 3D systems for investigating cell alignment and guidance cues for various cell types without mechanical force or other external stimulation, for a wide range of applications from tissue engineering to the control of cellular behaviors such as differentiation and function.

The freeze-drying process has been widely exploited for producing viable porous architectures for tissue engineering, mostly in case of polymer-based systems [24–29]. This technique does not require additional chemicals, relying instead on the water already present in solution/hydrogel to form ice crystals that can be sublimated from the polymer, creating a particular micro-architecture. The direction of growth and size of the ice crystals are a function of the temperature gradient and concentration of solution. By adjusting these parameters it is possible control the porosity and pore architecture [24, 26, 30–32].

In this work new silk fibroin 3D architectures with lamellar structures were successfully developed using a freeze-drying technique. We aimed at achieving a high degree of control over the lamellar morphology by varying silk solution concentration and freezing parameters. In order to induce stability of the scaffold morphology, different post-treatments were studied including methanol, water annealing and steam sterilization (autoclave). Human bone marrow-derived mesenchymal stem cells (hMSCs) grown under osteogenic conditions, were the selected cell population to investigate the suitability of the produced lamellar scaffolds for generating highly aligned 3D cell structures. Highly aligned structures as these can be found in the lamellar bone and also in the intervertebral disk (annulus fibrosus) [33]. To mimic such intricate systems is challenging and in the literature there are only a few examples of lamellar-like structures [28, 30, 34]. The freeze-drying methodology presented here generates highly reproducible SF lamellar structures with controlled spatial arrangement which is adequate for highly aligned 3D cell structures. The systems can find use in tissue engineering applications and constitute interesting substrates as models for investigating cell interactions and function in such highly oriented and confined spatial arrangements.

2. Materials & Methods

2.1 Preparation of lamellar scaffolds

Silk solution was prepared using *Bombyx mori* silkworm cocoons supplied by Tajima Shoji Co (Yokohama, Japan) according to protocols described in our previous studies [35, 36]. Briefly, cocoons of *B. mori* were boiled for 20 min. in an aqueous solution of 0.02 M sodium carbonate, and then rinsed thoroughly with pure water. After drying, the extracted silk fibroin was dissolved in a ternary solvent, $CaCl_2$-ethanol-water (1:2:8), at 60ºC for 3h, yielding a 20% (w/v) solution. This solution was dialyzed against distilled water using Slide-a-Lyzer dialysis cassettes (MWCO 3,500, Pierce) for 3 days to remove the salt. The final concentration of silk fibroin aqueous solution was approximately 8% (w/v). This concentration was determined by weighing the residual solid of a known volume of solution after drying. The solution was then diluted to obtain the following concentrations: 6, 4 and 2% (w/v). The different samples were cast into silicone molds, frozen at −80ºC overnight and freeze-dried (Telstar, Spain) for 2 days. Some of the samples were frozen at −5ºC for 4 hours prior to the described freeze-drying process. Samples with 7 mm in diameter and 4 mm in height were produced. In order to induce water-stability to the silk fibroin scaffolds, different procedures were used: i. Treatment with a methanol solution (90%) for 3 hours, ii. Water annealing [37] (briefly, the films were kept in a water-filled vacuumed desiccator at less than 10^{-3} mmHg for approximately 24 hours) and iii. Steam sterilization (120ºC, 15 psi, during 20 min; total cycle time: 1 hour). A scheme of the procedure is presented in figure 1.

2.2. Scanning Electron Microscopy (SEM)

The cross-sections of the lamellar scaffolds produced prior to and after the different treatments were examined by scanning electron microscopy (SEM). The samples were sputter coated with gold and examined with a LEO Gemini 982 Field Emission Gun SEM (Oberkochen, Germany).

2.3. Confocal and Multiphoton Microscopy

The different scaffolds were observed by Confocal and Multiphoton Microscopy. A confocal microscope (Bio-Rad MRC 1024, Hercules, CA) with Lasersharp 2000 software (excitation/emission 495/515 nm) was utilized for imaging. The region of interest was selected from z-plane images to include either the surface or the internal pores, beginning with a bottom section at least 1 mm above the surface of the scaffolds. Depth projection micrographs were obtained from 20 horizontal sections imaged at a depth distance of 50 mm from each other. Two-photon excited fluorescence (TPEF) images and spectra of the lamellar silk scaffolds were acquired at 755 and 800 nm excitation with a Leica TCS SP2 (Wetzlar, Germany) spectral confocal microscope equipped with a Mai-Tai Ti: Sapphire laser. The lamellar thickness (T) and interlamellar distance (ID) were calculated using the Leica Confocal Software according with figure 2. 10 measurements per condition were obtained.

2.4. Hydration degree

The degree of hydration of the porous constructs after the different treatments was investigated. All the samples were weighed before and after immersion in PBS (at 37ºC) for different time intervals up to one hour. At each time, the samples were removed from the flasks and immediately weighed to determine wet weight as function of the immersion time:

$$W_{absorbed} = \frac{(m_f - m_i)}{m_i} \times 100\% \quad \text{(Equation 1)}$$

Were m_i is the initial weight of the sample, and m_f is the sample wet weight after a given time of immersion.

2.5. Fourier Transformed Infrared Spectroscopy with Attenuated Total Reflectance (FTIR-ATR)

FTIR analysis of treated samples was performed in a Bruker Equinox 55/S FTIR spectrometer (Ettlingen, Germany), equipped with a deuterated triglycine sulfate detector and a multiple-reflection, horizontal MIRacle ATR attachment (using a Ge crystal, Pike Tech.). The instrument was continuously purged by nitrogen using blow-off from a liquid nitrogen tank to eliminate the spectral contributions of atmospheric water vapour. For each treated sample, a measurement of 66 scans was collected at a resolution of 4 cm^{-1}, which was acquired over a wavenumber range of 400–4,000 cm^{-1}. Spectral manipulations were performed with OPUS (Version 5.5 software, Bruker Optics, Inc.). Quantification of silk secondary structure was based on analyzing the amide I region (1,600–1,700 cm^{-1}) [38]. Background absorption due to water was subtracted from the sample spectra to obtain a flat recording in the range of 1,750–2,000 cm^{-1} [39]. The amide I region (1,600–1,710 cm^{-1}) was selected from the entire spectrum, and a linear baseline was applied to the spectrum. Deconvolution was carried out using 12 fixed fitting peak values as reported previously [40, 41]. To confirm that each fitting peak position represented a real spectral signal signature from the silk film sample, second derivative analysis was performed on spectra from each processing condition. Second derivative analysis was carried out using a third degree polynomial function with a 9-point Savitski-Golay smoothing function [39, 42]. During the deconvolution process, the peak positions were held constant for each sample to enable future comparisons between processing groups for protein secondary structure content. A Levenberg–Maquardt function available in the program was used for initial curve fitting. The curve fit was then refined using a local least squares fit, and the peak positions were reset to their initial positions if needed. The Levenberg–Maquardt function was used again for a final fit refinement. Throughout the process, the deconvoluted peak shapes were assumed to be Lorentzian [43]. The average percent composition of fibroin secondary structure for the series of samples [40, 44], specifically the amount of b-sheet structure was assessed by integrating the area of each deconvoluted curve and then normalizing to the total area of the amide I region of the fitted spectra.

2.6. Unconfined Compression Tests

Unconfined compression tests were performed on an Instron 3366 testing frame (USA) equipped with a 100N capacity load cell and custom-designed testing jig. Tests were conducted at room temperature in wet condition (soaking in PBS) and 5 samples were used per condition. A displacement control mode was used, with a crosshead displacement rate of 5 mm/min. The compressive stress and strain were graphed and yield strength as well as the compressive modulus and standard deviation determined. The elastic modulus was calculated based on a semi-automatic technique. The stress-strain diagram was segmented into 8 sections between the 0 and 10% strain range (starting at a 15N nominal tare load defined as 0% strain). Using least-squares' fitting, the highest slope among these 8 sections was defined as the compressive modulus for the sample. A line was drawn parallel to the modulus line, but offset by 2% of the sample gauge length. The corresponding stress value at which the offset line crossed the stress-strain curve was defined as the compressive yield strength of the scaffold.

2.7. Human Bone Marrow Stem Cell Isolation and Expansion

Total bone marrow (25 cm^3, Cambrex, Walkersville, MD) was diluted in 100 ml of medium (10% FBS) and prepared as previously reported [1]. In brief, cells were separated by density gradient centrifugation with 20 ml aliquots of bone marrow suspension overlaid onto a poly-

sucrose gradient (1077 g/cm^3, Histopaque, Sigma, St. Louis, MO) and centrifuged at 800x for 30 min at room temperature. Cells were pelleted and suspended in expansion medium (α-MEM, 10% FBS, 1 ng/ml bFGF, 100 U/ml penicillin, 100 mg/ml streptomycin, 0.25 mg/ml^{-1} fungizone, 0.1×10^{-3} M non-essential amino acids) and seeded in 75 cm^2 flasks at a density of 5×10^4 cells/cm^2. The adherent cells were allowed to reach approximately 80% confluence (12–17 d for the first passage). Cells were trypsinized, replated and passage 2 (P2) cells (80% confluence after 6–8 d), were used for the experiments.

2.8. *In Vitro* Culture

For examination of cell growth and differentiation in vitro on the silk scaffolds, P2 hMSCs (1×10^6 cells/scaffold) were seeded onto pre-wetted (a-MEM, overnight) scaffolds (7 mm diameter; 4 mm thick). 5 constructs per condition were placed into 6-well plates with osteogenic medium, placed in a humidified incubator at 37°C/5% CO_2. Medium was replaced at a rate of 50% every 2–3 d for 21 d. Osteogenic media consisted of α-MEM supplemented with 10% FBS, 0.1×10^{-3} M, non-essential amino acids, 50 μg/ml, ascorbic acid-2-phosphate, 10^{-8} M dexamethasone, 10×10^{-3} M β-glycerolphosphate and 1 μg/ml BMP-2 in the presence of 100 U/ml penicillin, 100 mg/ml streptomycin and 0.25 μg/ml fungizone.

Calcium Deposition Assay—Calcium deposition was assessed by Sigma Calcium Kit solution. Scaffolds samples were chopped into fine pieces in 500 ul 5% trichloraoacetic acid (TCA), and the supernatants were combined for assay according to the manufacturers' protocol. Results were read at 575 nm by VERSAmax microplate reader and normalized by the standards.

Pico Green DNA Quantification Assay and ALP Assay—DNA content and cell proliferation were assessed by Pico Green DNA Quantification Assay (Molecular Probes, city, state). Scaffold samples were chopped into fine pieces in 250 ul 0.2%Triton 100, and 80 ul were taken for Pico green assay. Samples were read at 480 nm/528 nm in a SpectraMas/GeminiEm fluorescence microplate reader and normalized by standards supplied by the kit. Alkaline phosphatase (ALP) activity was determined with an ALP kit from Sigma Diagnostics. A 120 ul aliquot of supernatant in 0.2% Triton was taken for ALP assay following the manufacturers' protocol. The conversion of p-nitrophenyl phosphate (colorless) to p-nitrophenol (yellow) was read at 405 nm in the same spectrometer as for the Picrogreen analysis. ALP activity was normalized by DNA content to display the ALP secreting amount per cell.

3. Results

3.1. Microstructural evolution of the scaffolds

Silk-based porous structures presenting different morphologies were successfully developed using a freeze-drying technique. Figure 3 presents a phase diagram indicating the influence of the solute concentration and initial freezing temperature on the resulting microstructure.

SF solutions at different concentrations were frozen at −80ºC. In this case, the effect of SF concentration on the resulting scaffold morphology was visualized from stage I to III. At low concentrations up to 4% (w/v) a fibrous structure was obtained (stage I). With increased concentration of SF, the microstructure gradually changed towards a lamellar morphology (III). SF solutions with a concentration of 8% (w/v) were frozen at −5ºC and −80ºC. The effect of the initial freezing temperature was observed by comparing stage III with IV. The morphology in this case changed into a globular shape when the freezing temperature was raised from −80°C to −5°C. For all the structures obtained, the pore morphology generated

after drying was a replica of the ice crystal shape that was formed during freezing. Therefore, to produce freeze-dried structures with controlled lamellar-like architecture, a stable dendritic ice crystal morphology without any side branches has to be formed during freezing [24, 26]. This effect was observed for concentrations higher than 6%, when SF solution presented a higher viscosity and for freezing temperatures of −80ºC. During the freezing process SF was rejected from the solidification front and concentrated in the non-crystallized channels between the plate-like dendrites, as illustrated in figure 3.

3.2. Structural integrity after inducing water stability

After optimizing the processing parameters towards a controlled lamellar morphology, scaffolds were produced from SF solutions with a concentration of 8% and submitted to different crystallization processes to induce water stability, namely a methanol treatment, water annealing and steam sterilization. The structural integrity of the scaffolds after the different crystallization methods is presented in figure 4.

Figure 4.a, b and c correspond to the original structure of the material, before any crystallization treatment. When comparing the different methods used for inducing water stability in the developed SF scaffolds it is possible to observe that both water annealing (figures 4.d, e and f) and methanol (figures 4.g, h and i) treatments induced some deformation in the lamellar structure. Some of the lamella collapsed, compromising the initial porosity of the construct. Additionally, in the case of methanol treatment a shrinkage of around 20%, was also observed as a result of the drying process. In the case of the water annealing treatment a swelling of the lamella was observed, due to the incorporation of water into the structure. When steam sterilization was used (figures 4j, k and l) the integrity of the lamellar structure was fully maintained. Besides the sterilization effect, this method was effective in preserving the original size and shape of the lamella and consequently, the constructs.

Figure 5 presents the average lamellar thickness and interlamellar distance of the scaffolds. Given the geometry of the pores it is more relevant to evaluate the appropriateness of the interlamellar distances to allow cell ingrowth than to evaluate the scaffold's porosity.

As presented in figure 5.a, the lamellar thicknesses were between 2,6 ± 0,3 μm for the methanol treated scaffolds and 5,8 ± 0,9 μm for water-annealed. These values are in the range of the reported for human lamellar bone which are between 3 to 5 μm thick [33]. When comparing the cross-section of the lamella before and after the different crystallization treatments it is possible to observe an increase in thickness after the water-based annealing procedure. This effect is consistent with observations by SEM (figure 4). As a result, the space between the lamella also increased (figure 5.b), indicating that during this process there was an expansion in the scaffold structure. When the methanol treatment was used a slight decrease in thickness was observed. During the drying process some of the lamella collapsed (figure 4.g, h, i) and therefore the interlamellar distance was variable and difficult to determine, also leading to high error bars. For the autoclaved scaffolds the thickness of the lamella did not vary and also the interlamellar distance did not change.

3.3. Chemical structure

Figure 6 shows the original FTIR spectra of the samples, before and after the different crystallization treatments. The assignment of the vibrational bands is made by reference to the literature, where comparable treatments to SF are reported for methanol [50], water annealing [42] and steam sterilization [51]. An example of a fitted spectrum of amide I with the individual deconvoluted peaks is also presented. Fourier transform self-deconvolution

was used to determine the fractional contributions to the FTIR amide I absorbance spectrum for the untreated samples in comparison with each crystallization treatment.

Table 1 lists the wavenumber ranges corresponding to the characteristic vibrational bands in *B. mori* silk, within the amide I region of the spectrum. The calculated values for the contributions to amide I are presented in Table 2, indicating the structural changes in the SF scaffolds induced by the different treatments.

As presented in figure 6.a the untreated freeze-dried scaffolds initially exhibited mostly an amorphous structure (1542 cm^{-1}) with silk I structure (1652 cm^{-1}). The majority of the silk matrix was composed of amorphous silk I structures (i.e., random coil, α-helix, and turn structures, in total ~91%). After the water annealing treatment, silk I was still predominant (1653 cm^{-1}), although the amount of β-sheet conformation increased from ~9 to ~24% (table 2). Upon exposure to methanol and steam sterilization, a peak shift was observed located at 1,626 and 1,625 cm^{-1}, respectively. In both cases such shifts indicate increased silk II β-sheet content with a simultaneous reduction of silk I content with bands in the range of 1,610–1,630 cm^{-1} region [40, 44]. In both cases the total β-sheet content increased to around 51% (figure 6.b, table 2). Similar values have been previously reported for both treatments [43, 45]. For steam sterilization treatment water vapor, and pressure promoted β-sheet crystallization to above 50%. The random coil and α-helix secondary structures exhibited the largest decrease in structure content for steam sterilized and methanol treatment, when compared to untreated and water annealed samples. While turn structures exhibited a decrease in structure content for methanol treated samples, this decrease was not significant in the case of the water vapor-mediated processes, i.e. water annealing and steam sterilization.

3.4. Compression properties

In figure 7 presents the mechanical behavior of the lamellar structures after the different crystallization methods after being subjected to unconfined compression forces.

When comparing the different crystallization methods both the stiffness and the compressive strength of the materials were affected. With the steam sterilization treatment there was a significant increase in both the stiffness and the strength of the materials when compared to the methanol treatment. The stiffness increased from 75,1 ± 25,2 to 290,0 ± 49,2 KPa while the strength increased from 10,8 ± 2,5 to 22,5 ± 3,1 KPa. This effect was the result of the application of the combined effect of water, temperature and pressure which did not allow for changes in the structure during the conformational changes that occurred in the material.

3.5. Degree of Hydration

The degree of hydration of the materials before and after the different crystallization treatments is represented in figure 8.

A higher degree of hydration was observed for the steam sterilization treatment, with mean values above 800%. Methanol treated samples also adsorbed similar amounts of PBS. In contrast, the degree of hydration achieved by the samples treated by the water-annealing process was considerably lower. Given the lamellar morphology of the scaffolds, the ability to hydrate is based on a capillary effect [46]. In the case of methanol, although a more hydrophobic structure was generated, the materials had more flexibility when immersed in PBS (as demonstrated in figure 7 by the lower mechanical properties in PBS). While the fluid was being adsorbed into the structure, the lamellas that were initially collapsed recovered their shape, allowing the structure to expand. This phenomena was observed by confocal microscopy, as presented in figure 9. Figure 9. AL Oliveira *et al.*

In this case, since there was sufficient re-alignment of the lamella an average lamellar distance of 20±6 μm was achieved (calculated for the structures immersed in PBS). In the case of the steam sterilization a high degree of hydration was also observed. Again a physical phenomenon seems to control the process. Although this structure presented the highest values for stiffness and strength the fact that the structure preserved its initial highly aligned morphology allowed for a higher absorption of PBS under the time frames evaluated.

3.6. Cell Morphology

To address the effect of the chemical structure and lamellar morphology on the biological response of the materials, hMSCs were seeded on the scaffolds treated with methanol (highest β-sheet content, lowest lamellar thickness, high hydration degree) and by the water annealing process (lowest β-sheet content, highest lamellar thickness, low hydration degree). Two-photon excited fluorescence (TPEF) images were acquired, as presented in figure 10. TPEF images revealed in green the lamellar morphology obtained after freeze-drying and subsequent stabilization treatments of methanol (figure 10.a) and water annealing (figure 10.b). The presence of collagen on the constructs cultured after 3 weeks, based on Second Harmonic Generation, is presented in red (figures 10.c and 9.d). Collagen is aligned with the lamella, particularly in the case of the methanol treatment. The lamellar morphology constituted a patterned surface onto which hMSCs attached and proliferated and guided the formation of the extracellular matrix. SEM analysis was performed to the cross-section of the scaffolds after cell culture for 3 weeks (figure 11).

For the methanol treated lamellar scaffolds, the presence of extracellular matrix was observed along 4 mm of the scaffold's cross-section, which indicates that the cells were able to migrate through the spaces between the lamella to the innermost region of the scaffolds. The scaffolds with this thickness and using methanol treatment therefore presented good interconnectivity as it was possible to obtain layers of cells/ECM intercalated with the SF lamellas in a multi-layer assembly. In the case of the water annealed scaffolds this effect was not observed. Since the materials were not able to fully expand in solution many of the layers remained collapsed, which compromised the overall interconnectivity.

3.7. Biochemical analysis

Figure 12 presents the biochemical characterization of a) ALP, b) DNA and c) Ca^{2+}, for hMSCs cells cultured up to 6 weeks. Figure 12. AL Oliveira *et al.*

The DNA content of the lamellar silk constructs was measured to quantify cell proliferation. The cell number after 1 day of seeding was higher in the water annealed scaffolds as compared with those treated with methanol ($p<0.05$). This can be explained by a difference in the seeding efficiency. In the scaffolds treated with methanol the cells could easily penetrate between the lamella, some being lost to the bottom of the well.. In water annealed scaffolds the cells were mostly located at its surface, since the structure is more dense. After 42 days of culture the cell number, as determined by DNA content, was significantly higher for water annealed scaffolds (figure 12.a). This result indicates that at this stage, the differences in the chemical structure, mechanical properties and morphology of the constructs were relevant to stimulate cell proliferation. Still, one has to consider that in the water annealed scaffolds most of the cells were located at the surface of the scaffolds having better access to oxygen and nutrients supply from the medium, which can have a consequence in the resulting cell number.

ALP activity was determined for up to 42 days of culture (figure 12.b). This biochemical assay is a marker of early osteoblastic differentiation and commitment of bone marrow stem

cells toward the osteoblastic phenotype [47]. As expected, in the first 21 days there was a gradual increase in ALP in both the scaffolds treated with methanol and with water annealing. There were no significant differences between the values obtained for the scaffolds treated with these procedures, although the mean values were consistently higher for the water annealing process. After 42 days this difference became significant ($p<0.05$). To determine mineralized matrix deposition in the lamellar scaffolds a calcium dissolution assay was conducted (figure 12.c). During the first 21 days there were no differences between the amount of mineralized matrix deposited in the methanol treated scaffolds as compared to those treated by the water annealed process. However, at day 42 it was possible to observe an increase in Ca^{2+} for the water annealed scaffolds indicating that in this environment cells were able to produce more mineralized matrix.

4. Discussion

Control of the microstructure of ice formation

It has been well established that the microstructural features obtained during freeze-drying are mainly controlled by exploiting the physics of ice formation [24, 26, 34, 48]. In the present study, by controlling parameters such as the freezing temperature and the concentration of the silk solution it was possible to modulate the morphology of the ice crystals to generate anisotropic porous scaffolds with a regular lamellar morphology. For the lowest freezing temperature used (−80ºC) a preferential growth direction was imposed to the ice crystals, which reflected in a highly oriented porous morphology. As previously described [26], the solidification occurs under a steady-state freezing regime where the ice crystals exhibit a homogeneous morphology without any side branches throughout the construct. The growing ice crystals reject the dissolved silk and transfer heat from the moving interface of ice-water into the remaining unfrozen water. Under these conditions of directional freezing, the solution concentrates in the phases between the growing ice crystals and an advancing solid/liquid interface is created [48]. The influence of the freezing rate on pore structure has been studied for collagen-based scaffolds [49], where the formation of ice crystals within the protein suspension was influenced by both the rate of nucleation of ice crystals and the rate of heat and protein diffusion.

Recently, there has been interest in the production of highly aligned polymeric structures, given their application potential. Directional freezing has been investigated as a simple strategy for the preparation of controlled aligned polymeric structures [27, 29–31, 34, 50–53]. This process is based on traditional freeze-drying, although it allows for controlling the movement of the freezing front, thereby creating well-structured materials with fewer defects. Aqueous polymer solutions, colloids, or their mixtures have been aligned to form biomimetic structures for engineering tissues such as cartilage [28, 52], peripheral nerves and the spinal cord [27–29, 31, 50, 53]. In a work by Stokols *et al.* [29] freeze-dry processing was used to create scaffolds from agarose, with uniaxial linear pores. Khang et al. [50] used freeze-drying for fabrication tubular porous poly(L-lactide- co-glycolide) structures. Spector *et al.* [31] developed cylindrical collagen-based scaffolds also axially oriented pore channels. Gao *et al.* [28] proposed new porous gelatin scaffolds with microtubule orientation using a unidirectional freeze-drying technology. Matrices with this porous structure have potential to improve the regeneration of tubular organ structures such as peripheral nerves and the spinal cord by physically supporting and guiding the growth of neural structures across the site of injury. Matrices with a lamellar-like structure can find applications for lamellar bone and also in the intervertebral disk (Annulus fibrosus) regeneration. However, freeze-dried lamellar-like structures are not easy to obtain. To our knowledge, only few studies have reported the development of such architectures [30, 32, 54]. The major difficulty encountered is to achieve enough control during ice formation to avoid the formation of lamellar structures with defects, as those observed for instances in the

morphologies reported by Gao *et al.* [28] and Kang *et al.* [54] for gelatin scaffolds or by *Deville et al.* [24] for hydroxyapatite slurries. Waschkies and co-workers [55] developed a procedure to control the freezing process of alumina suspensions using a double-side cooling method. Using this setup and theoretical knowledge, they were able to control microstructure development over several centimeters. Nevertheless, some defects were observed.

The processing route proposed in the present work was effective in generating defect-free lamellar-like morphology with very regular lamellar thickness and interlamellar distance. In our case, directional freezing was achieved by adjusting the freezing temperature, considering the cylinder geometry and scaffold volume. This morphology is known to improve the mechanical properties while reducing volume density, leading to unusually high compressive strength [24].

Effect of the water stabilization treatment

Different crystallization processes were proposed to induce water stability of the scaffolds. As expected, the methanol treatment was effective in generating β-sheets. A decrease in the thickness was observed, due to a contraction effect during transition to β-sheet conformation. Also, the materials suffered shrinkage during methanol evaporation due to capillary forces and stress development between lamella, from the surface to the center during drying. Nevertheless, when re-hydrated, the collapsed lamellae were able to realign and recover to some extent their initial shape. Water annealing treatment also induced some distortion to the lamellar structure combined with an increase of the thickness of the layers. This structural adjustment can be explained by the increase in mobility of the silk fibroin chains due to the absorption of water and a decrease in the glass transition temperature (Tg), attributed to water molecules behaving as a plasticizer to allow greater intermolecular movement between fibroin protein chains [56–58]. Under these supersaturated conditions of humidity a phase transition occurs and the random coil form of silk fibroin is stabilized by hydration to yield a silk I structure [37]. When immersed in PBS solution, water annealed constructs were not able recover the initial lamellar alignment

Steam sterilization was effective in inducing β-sheet conformation without introducing dimensional variations to the scaffolds' morphology. Lawrence *et al.* [59] first introduced this treatment as a viable solvent-free methodology for water stability of cast SF membranes for corneal regeneration. In this work we evaluated the suitability of this process to stabilize 3D porous architectures, without compromising structural integrity. This treatment is inspired by the same principles as the water annealing process, however it has the advantage of combining the effect of pressure and temperature to accelerate conformational changes, from the silk I to the more energetically favorable silk II state, thereby promoting more β-sheet formation. Hu *et al.* [58] have studied the mechanism of structural evolution of SF during water annealing samples at different temperatures (4–100 ºC). According to their model, for the highest temperature studied the water vapor molecules will bring thermal energy into the protein-bound water system and the kinetics of crystal growth will increase. Considering the steam-sterilization treatment, this effect will be catalyzed by the presence of pressure in the system. In this way, higher crystallinity can be reached within a shorter time. The compressive stiffness and the strength of the resulting lamellar structures were significantly enhanced with this treatment as compared to methanol or water-annealing.

The hydration capacity of the stabilized SF materials results from the combined effect of the surface properties with the bulk mechanical properties. The capillarity effect is a well-known phenomenon which is dependent on the surface wettability [46]. Methanol treatment generates a higher content of β-sheet domains, which are hydrophobic. In contrast, water-annealed scaffolds will be more hydrophilic. As reported, the contact angle of SF increases

from 62,6 after water annealing to 71,4 for methanol treated. In the case of the steam sterilization treatment the contact angle value should be close to the methanol treated surfaces, given the similar amount of β-sheet content. Therefore, it would be expected that the more hydrophilic materials, i.e. those treated by the water-annealing process, should exhibit a higher degree of hydration. From the materials chemistry perspective, the results seem contradictory. However, in this case the contribution of physical effects, such as the available interlamellar space and the mechanical properties exhibited by the materials when immersed in PBS, resulted in different outcomes concerning the capacity of fluid absorption. The water-annealed structures with a higher chemical affinity to water and already some degree of expansion, presented the lowest degree of hydration. This result was higher resistance to dimensional change, as demonstrated by the mechanical performance during compression. These features likely did not allow for the full expansion of the structure when in contact with PBS for 60 minutes. For the steam sterilization treatment, since the structural integrity of the materials were not compromised, the spaces between lamella did not changed, which favoured the hydration process. This treatment was the most suitable for inducing water stability while having the advantage of sterilizing the materials.

In vitro cell behavior and spatial organization

The biochemical results revealed that in scaffolds treated by the water annealing process there was an increase in cell proliferation and subsequent ECM production [47]. This phenomena has been reported previously, comparing water annealed membranes with those treated with methanol [37]. In this case the differences in protein conformation and consequently in Silk II content, crystallinity and wettability of the surface, were the main factors associated with different cell behaviour.

The different morphological features such as the lamellar thickness or interlamellar distance seem also to be responsible for the differences in cell activity. The lamellar constructs allowed hMSCs to attach and proliferate, guiding the formation of extracellular matrix after 21 days of cell culture. For water annealed scaffolds the cells aligned mostly at the surface, which served as a pattern for cells to attach and proliferate for guiding matrix deposition. In the case of methanol treated scaffolds, after immersion in culture medium significant recovery of the initial morphology was observed due to a re-alignment of the lamella. This increase in interlamellar space allowed hMSCs to attach, proliferate and align, progressing to the interior of the scaffold. Under this spatial confinement these cells were able to produce highly aligned collagen matrix alternated with the SF lamella in a multi-layer assembly. This kind of cell alignment following the morphology of the material can be useful in generating tissues with highly anisotropic properties. In this work we envisioned lamellar bone as a possible target application for these highly aligned laminated structures. However, given the ability of these structures to hydrate, several other applications can also be envisioned such as for cartilage [27, 28, 52]. As reported by Woo *et al.* [60] the importance of cell alignment in several biological tissues is to optimization of function. Cell-matrix interactions are paramount for the successful repair and regeneration of damaged and diseased tissue. Since many tissues have an anisotropic architecture, it has been proposed that aligned extracellular matrix (ECM) could guide and support the differentiation of resident MSCs [60–62]. Our results give some insight on the regulation of hMSCs through directional ECM structures and demonstrate the potential of these 3D lamellar structures as cell culture platforms for guiding the morphogenesis of anisotropic tissues. In addition, the preparation of highly aligned structures with aligned porosity in the micrometer range can be of technological importance for a wide range of other applications, such organic electronics, microfluidics and molecular filtration, among others.

5. Conclusions

A simple methodology for designing new silk fibroin materials with controlled lamellar morphology is presented. Steam sterilization was a suitable method for inducing water stability, preserving the structural integrity and improving mechanical properties, while also sterilizing the constructs. Methanol treated scaffolds presented an adequate interlamellar distance for cell migration, resulting in the formation of layers of cells/ECM intercalated with the SF. Therefore, the lamellar morphology obtained allowed hMSCs to attach and proliferate, guiding the formation of extracellular matrix. The results offer interesting possibilities for developing highly aligned structures and for the engineering of specific tissues were anisotropic properties are desirable.

Acknowledgments

A.L. Oliveira wishes to thank financial support from the Portuguese Foundation for Science and Technology (SFRH/BPD/39102/2007) under POCTI Program. This work was partially supported by FCT through POCTI and/or FEDER programs and by the NIH [DE017207, EB003210 and EB002520].

References

1. Altman GH, Diaz F, Jakuba C, Calabro T, Horan RL, Chen JS, et al. Silk-based biomaterials. Biomaterials. 2003; 24:401–16. [PubMed: 12423595]
2. Kaplan DL, Numata K, Cebe P. Mechanism of enzymatic degradation of beta-sheet crystals. Biomaterials. 2010; 31:2926–33. [PubMed: 20044136]
3. Jiang CY, Wang XY, Gunawidjaja R, Lin YH, Gupta MK, Kaplan DL, et al. Mechanical properties of robust ultrathin silk fibroin films. Adv Funct Mater. 2007; 17:2229–37.
4. Meinel L, Uebersax L, Hagenmueller H, Hofmann S, Gruenblatt E, Mueller R, et al. Effect of scaffold design on bone morphology in vitro. Tissue Engineering. 2006; 12:3417–29. [PubMed: 17518678]
5. Altman GH, Horan RL, Lu HH, Moreau J, Martin I, Richmond JC, et al. Silk matrix for tissue engineered anterior cruciate ligaments. Biomaterials. 2002; 23:4131–41. [PubMed: 12182315]
6. Chang G, Kim HJ, Kaplan D, Vunjak-Novakovic G, Kandel RA. Porous silk scaffolds can be used for tissue engineering annulus fibrosus. Eur Spine J. 2007; 16:1848–57. [PubMed: 17447088]
7. Chao PHG, Yodmuang S, Wang XQ, Sun L, Kaplan DL, Vunjak-Novakovic G. Silk hydrogel for cartilage tissue engineering. J Biomed Mater Res B. 2010; 95B:84–90.
8. Enomoto S, Sumi M, Kajimoto K, Nakazawa Y, Takahashi R, Takabayashi C, et al. Long-term patency of small-diameter vascular graft made from fibroin, a silk-based biodegradable material. J Vasc Surg. 2010; 51:155–64. [PubMed: 19954921]
9. Kaplan DL, Omenetto FG. New Opportunities for an Ancient Material. Science. 2010; 329:528–31. [PubMed: 20671180]
10. Kaplan DL, Mandal BB, Park SH, Gil ES. Multilayered silk scaffolds for meniscus tissue engineering. Biomaterials. 2011; 32:639–51. [PubMed: 20926132]
11. Reis RL, Gomes S, Leonor IB, Mano JF, Kaplan DL. Spider silk-bone sialoprotein fusion proteins for bone tissue engineering. Soft Matter. 2011; 7:4964–73.
12. Silva SS, Motta A, Rodrigues MT, Pinheiro AFM, Gomes ME, Mano JF, et al. Novel Genipin-Cross-Linked Chitosan/Silk Fibroin Sponges for Cartilage Engineering Strategies. Biomacromolecules. 2008; 9:2764–74. [PubMed: 18816100]
13. Bessa PC, Balmayor ER, Cerqueira MT, Rada T, Gomes ME, Neves NM, et al. Silk nanoparticles for delivery of human BMP-2 in bone regenerative medicine applications. Tissue Eng Pt A. 2008; 14:776–7.
14. Ramakrishna S, Liao S, Chan CK. Stem cells and biomimetic materials strategies for tissue engineering. Mat Sci Eng C-Bio S. 2008; 28:1189–202.
15. Khademhosseini A, Wheeldon I, Farhadi A, Bick AG, Jabbari E. Nanoscale tissue engineering: spatial control over cell-materials interactions. Nanotechnology. 2011:22.

16. Hutmacher DW, Sittinger M, Risbud MV. Scaffold-based tissue engineering: rationale for computer-aided design and solid free-form fabrication systems. Trends Biotechnol. 2004; 22:354–62. [PubMed: 15245908]

17. Mano JF, Alves NM, Pashkuleva I, Reis RL. Controlling Cell Behavior Through the Design of Polymer Surfaces. Small. 2010; 6:2208–20. [PubMed: 20848593]

18. Pirraco RP, Marques AP, Reis RL. Cell interactions in bone tissue engineering. Journal of Cellular and Molecular Medicine. 2010; 14:93–102. [PubMed: 20050963]

19. Kang CE, Gemeinhart EJ, Gemeinhart RA. Cellular alignment by grafted adhesion peptide surface density gradients. J Biomed Mater Res A. 2004; 71A:403–11. [PubMed: 15481057]

20. Levenberg S, Dado D. Cell-scaffold mechanical interplay within engineered tissue. Seminars in Cell & Developmental Biology. 2009; 20:656–64. [PubMed: 19596326]

21. Chung JH, Kim JH, Cho CS, Choung YH, Lim KT, Son HM, et al. Mechanical Stimulation of Mesenchymal Stem Cells for Tissue Engineering. Tissue Eng Regen Med. 2009; 6:199–206.

22. Vunjak-Novakovic G, Tandon N, Cannizzaro C, Chao PHG, Maidhof R, Marsano A, et al. Electrical stimulation systems for cardiac tissue engineering. Nat Protoc. 2009; 4:155–73. [PubMed: 19180087]

23. Torbet J, Malbouyres M, Builles N, Justin V, Roulet M, Damour O, et al. Orthogonal scaffold of magnetically aligned collagen lamellae for corneal stroma reconstruction. Biomaterials. 2007; 28:4268–76. [PubMed: 17618680]

24. Deville S, Saiz E, Nalla RK, Tomsia AP. Freezing as a path to build complex composites. Science. 2006; 311:515–8. [PubMed: 16439659]

25. Zmora S, Glicklis R, Cohen S. Tailoring the pore architecture in 3-D alginate scaffolds by controlling the freezing regime during fabrication. Biomaterials. 2002; 23:4087–94. [PubMed: 12182310]

26. Schoof H, Bruns L, Fischer A, Heschel I, Rau G. Dendritic ice morphology in unidirectionally solidified collagen suspensions. J Cryst Growth. 2000; 209:122–9.

27. Lee J, Lee MK, Chung NO. Membranes with through-thickness porosity prepared by unidirectional freezing. Polymer. 2010; 51:6258–67.

28. Gao J, Wu X, Liu Y, Li X, Wen P, Zhang Y, et al. Preparation of aligned porous gelatin scaffolds by unidirectional freeze-drying method. Acta biomaterialia. 2010; 6:1167–77. [PubMed: 19733699]

29. Stokols S, Tuszynski MH. The fabrication and characterization of linearly oriented nerve guidance scaffolds for spinal cord injury. Biomaterials. 2004; 25:5839–46. [PubMed: 15172496]

30. Schoof H, Apel J, Heschel I, Rau G. Control of pore structure and size in freeze-dried collagen sponges. J Biomed Mater Res. 2001; 58:352–7. [PubMed: 11410892]

31. Spector M, Madaghiele M, Sannino A, Yannas IV. Collagen-based matrices with axially oriented pores. J Biomed Mater Res A. 2008; 85A:757–67. [PubMed: 17896767]

32. Deville S. Freeze-casting of porous ceramics: A review of current achievements and issues. Adv Eng Mater. 2008; 10:155–69.

33. Weiner S, Traub W, Wagner HD. Lamellar bone: Structure-function relations. Journal of Structural Biology. 1999; 126:241–55. [PubMed: 10475685]

34. Zhang HF, Hussain I, Brust M, Butler MF, Rannard SP, Cooper AI. Aligned two- and three-dimensional structures by directional freezing of polymers and nanoparticles. Nat Mater. 2005; 4:787–93. [PubMed: 16184171]

35. Kim HJ, Kim HS, Matsumoto A, Chin IJ, Jin HJ, Kaplan DL. Processing windows for forming silk fibroin biomaterials into a 3D porous matrix. Aust J Chem. 2005; 58:716–20.

36. Kim HJ, Kim UJ, Leisk GG, Bayan C, Georgakoudi I, Kaplan DL. Bone regeneration on macroporous aqueous-derived silk 3-D scaffolds. Macromolecular Bioscience. 2007; 7:643–55. [PubMed: 17477447]

37. Jin HJ, Park J, Karageorgiou V, Kim UJ, Valluzzi R, Kaplan DL. Water-stable silk films with reduced beta-sheet content. Adv Funct Mater. 2005; 15:1241–7.

38. Arrondo JLR, Prado A, Echabe I, Goni FM. Protein Conformational-Changes Induced by Surfactants as Studied by Ft-Ir. Biophysical Journal. 1993; 64:A382–A.

39. Dong A, Huang P, Caughey WS. Protein Secondary Structures in Water from 2nd-Derivative Amide-I Infrared-Spectra. Biochemistry. 1990; 29:3303–8. [PubMed: 2159334]
40. Tretinnikov ON, Tamada Y. Influence of casting temperature on the near-surface structure and wettability of cast silk fibroin films. Langmuir. 2001; 17:7406–13.
41. Hu X, Kaplan D, Cebe P. Determining beta-sheet crystallinity in fibrous proteins by thermal analysis and infrared spectroscopy. Macromolecules. 2006; 39:6161–70.
42. Speare JO, Rush TS. IR spectra of cytochrome c denatured with deuterated guanidine hydrochloride show increase in beta sheet. Biopolymers. 2003; 72:193–204. [PubMed: 12722115]
43. Matsumoto A, Chen J, Collette AL, Kim UJ, Altman GH, Cebe P, et al. Mechanisms of silk fibroin sol-gel transitions. Journal of Physical Chemistry B. 2006; 110:21630–8.
44. Wilson D, Valluzzi R, Kaplan D. Conformational transitions in model silk peptides. Biophysical Journal. 2000; 78:2690–701. [PubMed: 10777765]
45. Cebe P, Hu X, Kaplan D. Determining beta-sheet crystallinity in fibrous proteins by thermal analysis and infrared spectroscopy. Macromolecules. 2006; 39:6161–70.
46. Israelachvili JN, Mcguiggan PM. Forces between Surfaces in Liquids. Science. 1988; 241:795–800. [PubMed: 17829174]
47. Stein GS, Lian JB, Owen TA, Bortell R, Vanwijnen AJ, Bidwell JP, et al. Integrated Relationship of Proliferation and Differentiation during Osteoblast Phenotype Development. Frontiers of Osteosarcoma Research. 1993:387–401. 570.
48. Butler MF. Freeze concentration of solutes at the ice/solution interface studied by optical interferometry. Crystal Growth & Design. 2002; 2:541–8.
49. O'Brien FJ, Harley BA, Yannas IV, Gibson L. Influence of freezing rate on pore structure in freeze-dried collagen-GAG scaffolds. Biomaterials. 2004; 25:1077–86. [PubMed: 14615173]
50. Khang G, Jeon JH, Cho JC, Lee HB. Fabrication of tubular porous PLGA scaffold by emulsion freeze-drying method. Polym-Korea. 1999; 23:471–7.
51. Kim G, Ahn S, Kim Y, Cho Y, Chun W. Coaxial structured collagen-alginate scaffolds: fabrication, physical properties, and biomedical application for skin tissue regeneration. J Mater Chem. 2011; 21:6165–72.
52. Liu Y, Wen P, Gao JP, Zhang YL, Li XL, Long Y, et al. Fabrication of Chitosan Scaffolds with Tunable Porous Orientation Structure for Tissue Engineering. J Biomat Sci-Polym E. 2011; 22:19–40.
53. Sannino A, Madaghiele M. Tuning the Porosity of Collagen-based Scaffolds for Use as Nerve Regenerative Templates. J Cell Plast. 2009; 45:137–55.
54. Kang HW, Tabata Y, Ikada Y. Fabrication of porous gelatin scaffolds for tissue engineering. Biomaterials. 1999; 20:1339–44. [PubMed: 10403052]
55. Waschkies T, Oberacker R, Hoffmann MJ. Control of Lamellae Spacing During Freeze Casting of Ceramics Using Double-Side Cooling as a Novel Processing Route. J Am Ceram Soc. 2009; 92:S79–S84.
56. Cebe P, Hu X, Kaplan D. Effect of water on the thermal properties of silk fibroin. Thermochim Acta. 2007; 461:137–44.
57. Agarwal N, Hoagland DA, Farris RJ. Effect of moisture absorption on the thermal properties of Bombyx mori silk fibroin films. J Appl Polym Sci. 1997; 63:401–10.
58. Kaplan DL, Hu X, Shmelev K, Sun L, Gil ES, Park SH, et al. Regulation of Silk Material Structure by Temperature-Controlled Water Vapor Annealing. Biomacromolecules. 2011; 12:1686–96. [PubMed: 21425769]
59. Kaplan DL, Lawrence BD, Omenetto F, Chui K. Processing methods to control silk fibroin film biomaterial features. J Mater Sci. 2008; 43:6967–85.
60. Woo SLY, Almarza AJ, Yang GG, Nguyen T, Abramowitch SD. Positive changes in bone marrow-derived cells in response to culture on an aligned bioscaffold. Tissue Eng Pt A. 2008; 14:1489–95.
61. Ye JD, Qi XP, Wang YJ. Alginate/poly (lactic-co-glycolic acid)/calcium phosphate cement scaffold with oriented pore structure for bone tissue engineering. J Biomed Mater Res A. 2009; 89A:980–7. [PubMed: 18470921]

62. Werner C, Lanfer B, Seib FP, Freudenberg U, Stamov D, Bley T, et al. The growth and differentiation of mesenchymal stem and progenitor cells cultured on aligned collagen matrices. Biomaterials. 2009; 30:5950–8. [PubMed: 19674785]

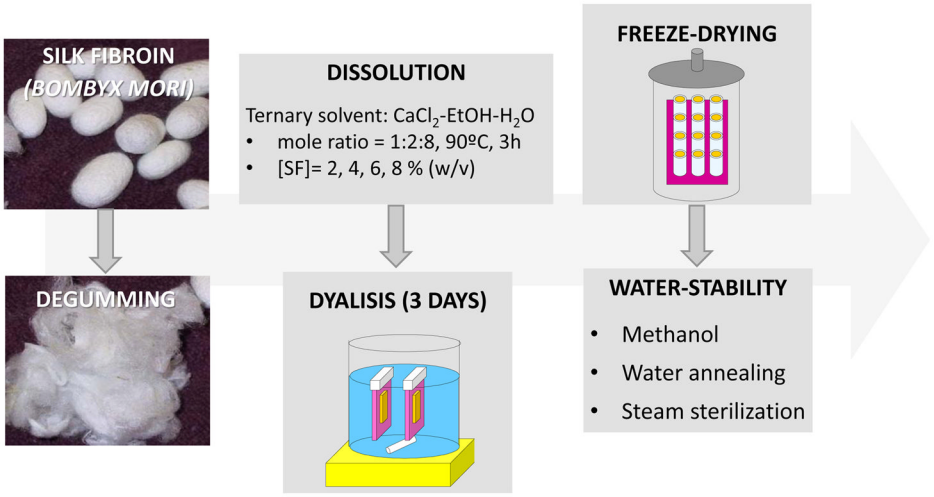

Figure 1.
Schematic drawing of the procedure to produce the SF lamellar scaffolds.

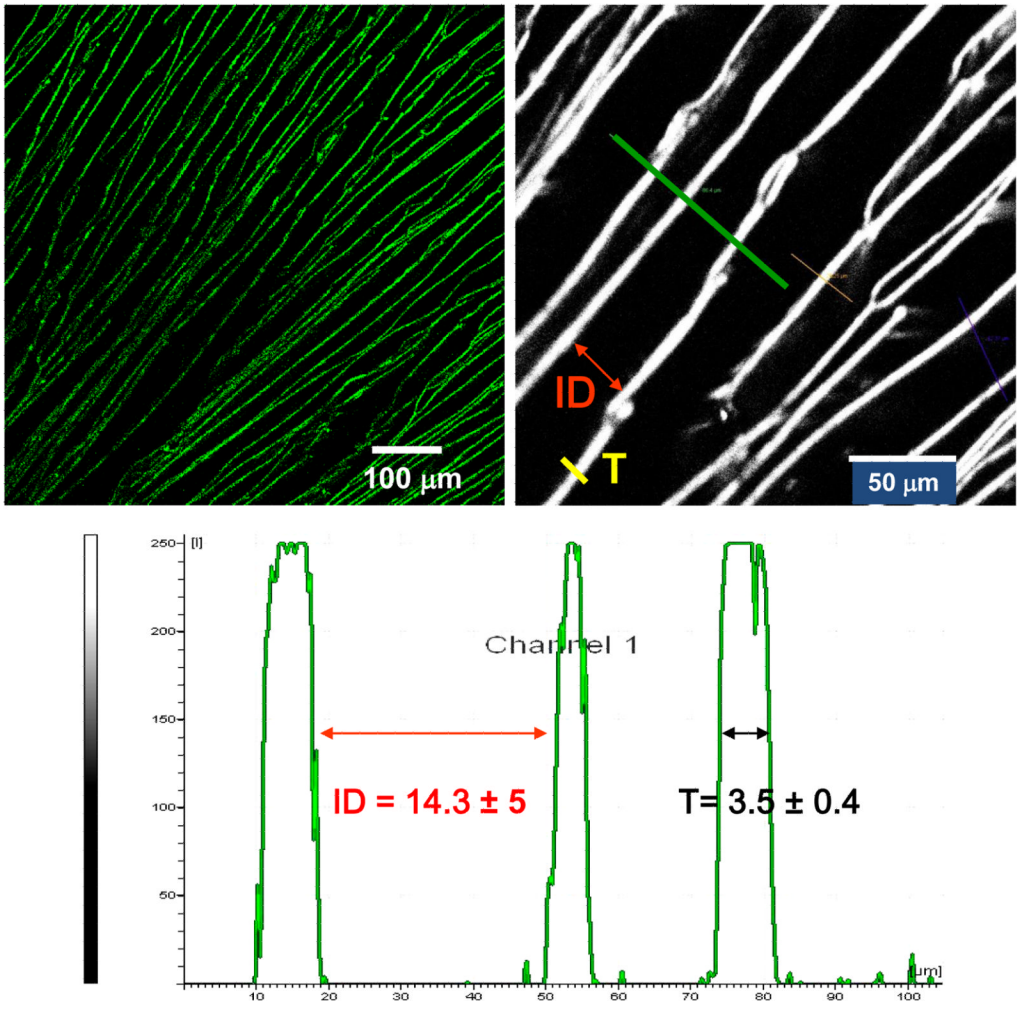

Figure 2.
Example of images obtained during microstructural analysis using two-photon excited fluorescence and profile obtained for the calculation of the lamellar thickness (T) and interlamellar distance (ID).

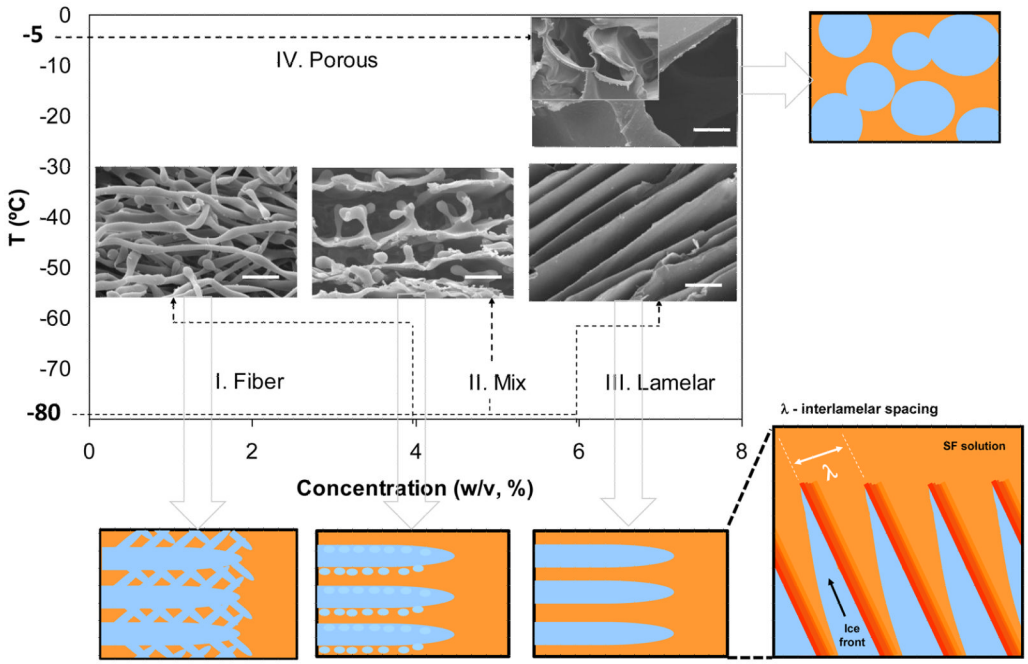

Figure 3.
Microstructural evolution of the SF scaffolds produced by freeze-drying. Scale bar: 10 μm.

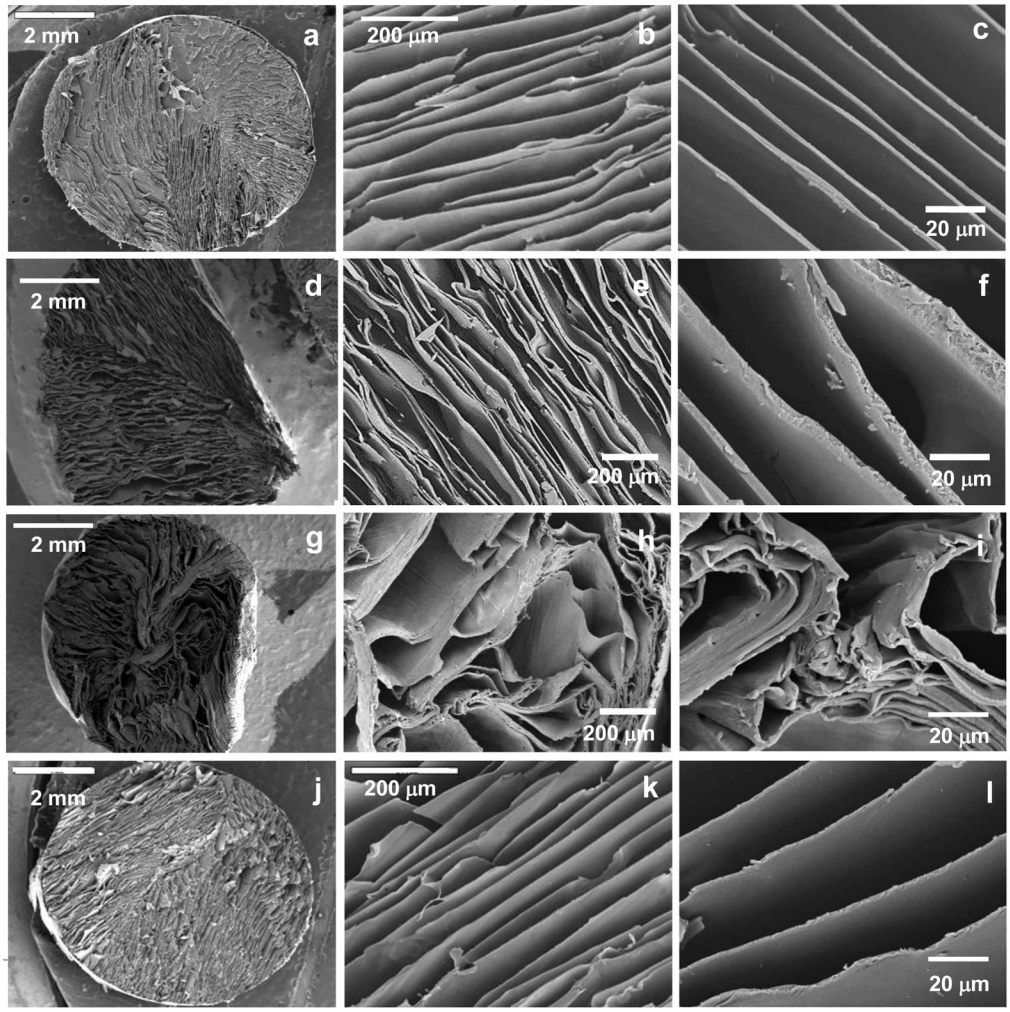

Figure 4.
SEM micrographs showing the morphology of the cross-sections of the scaffolds (a,b,c) untreated and after the different crystallization methods: (d,e,f) methanol treatment, (g,h,i) water annealing and (j,k,l) steam sterilization.

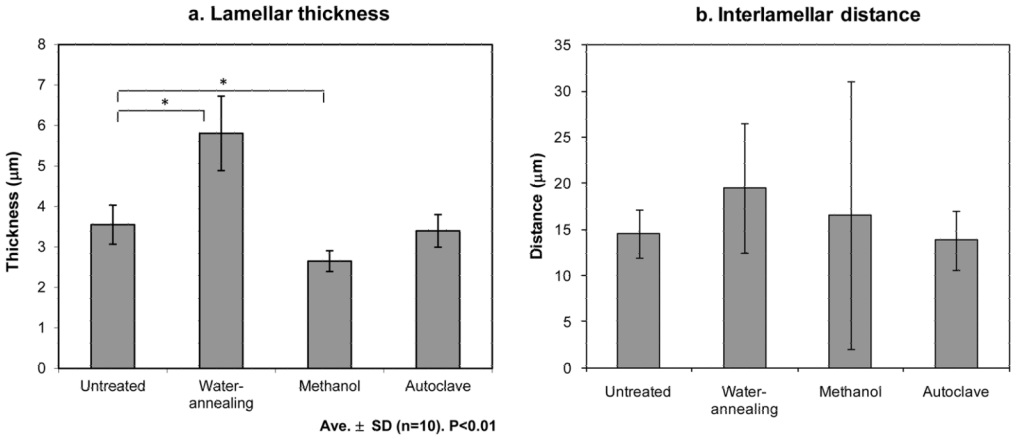

Figure 5.

Average lamellar thickness (a) and interlamellar distance (b) of the scaffolds untreated and after the different crystallization methods.

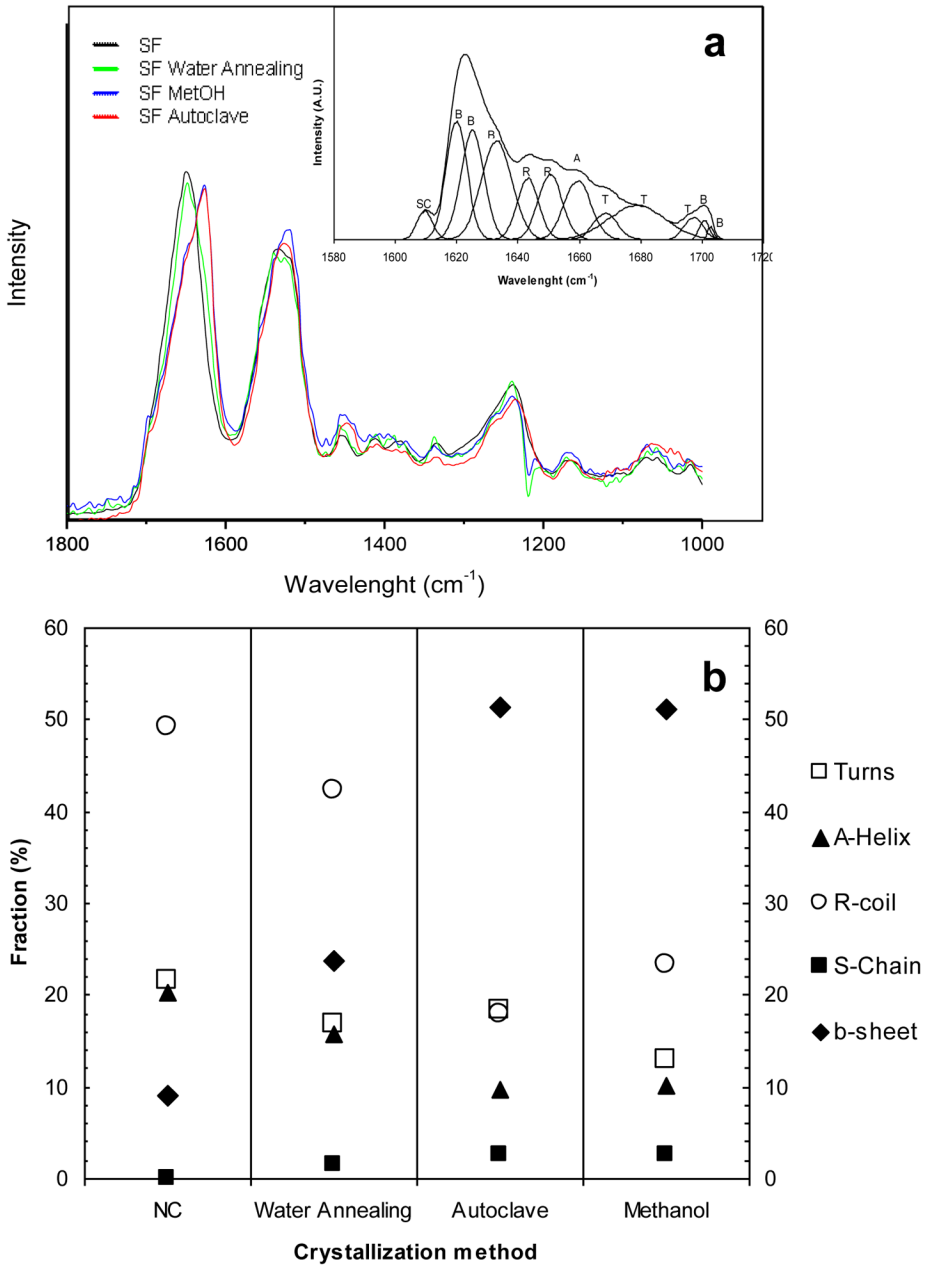

Figure 6.

(a)FTIR absorbance spectra in the region of amide I (1,600–1,700 cm^{-1}) and amide II (1,500–1,600 cm^{-1}), obtained as function of the crystallization treatment performed to the lamellar scaffolds; example of an absorbance spectra of amide I, deduced after Fourier self-deconvolution. (b) Fractional contributions to the FTIR amide I absorbance spectrum, determined by Fourier transform self-deconvolutionvs crystallization treatment. The contributions to the amide I band are marked as: ○ random coil (R), ◆beta-sheets (B), ▲ alpha-helices (A), □ turns (T), and ■side chains (SC).

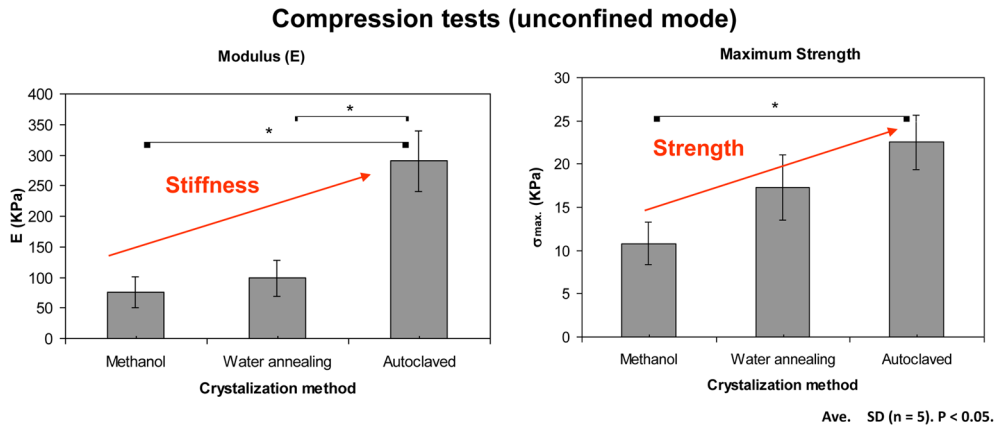

Figure 7.
Mechanical behaviour under compression of the lamellar structures after the different crystallization treatments.

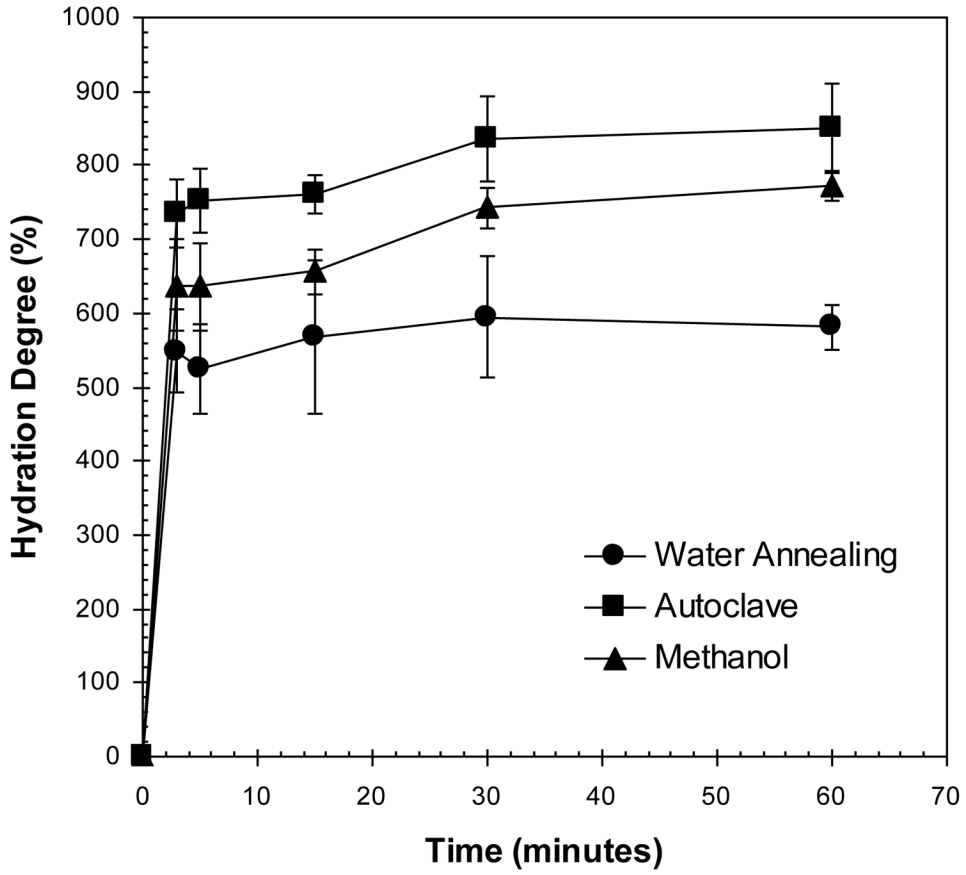

Figure 8.
Degree of hydration of the lamellar structures after immersion in PBS (at 37ºC).

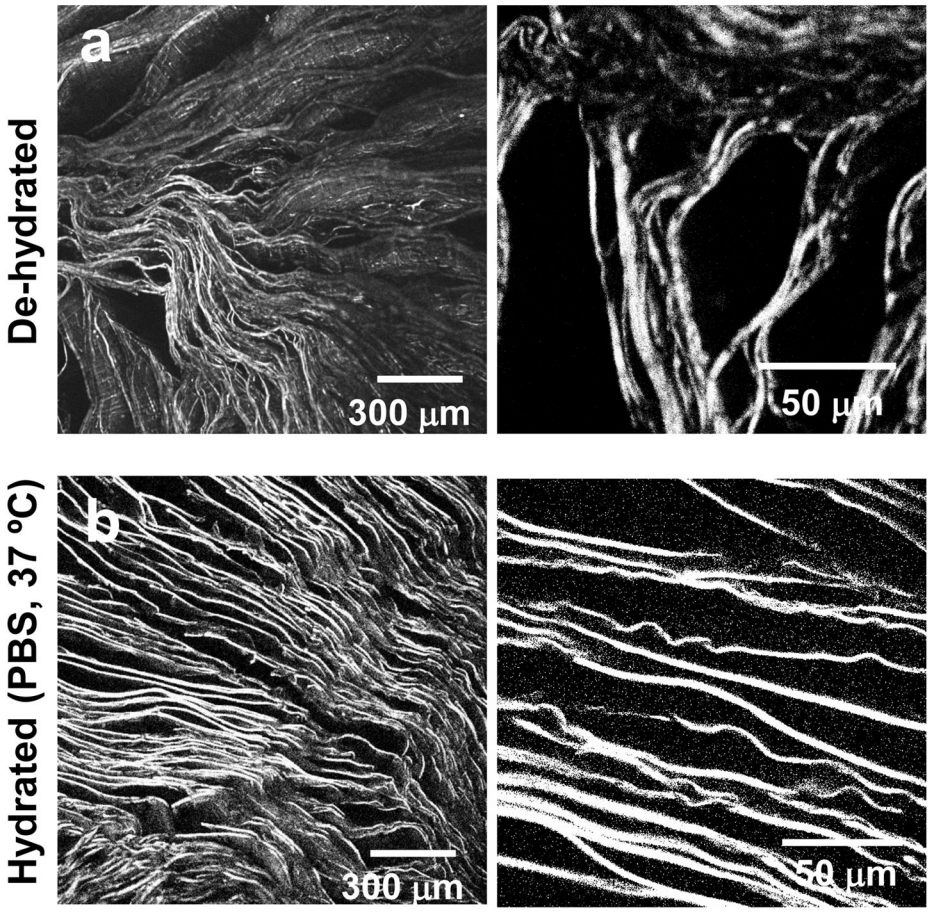

Figure 9.
Confocal micrographs of a) the lamellar scaffolds dried after the methanol treatment and b) after subsequent re-hydration in PBS solution at 37ºC.

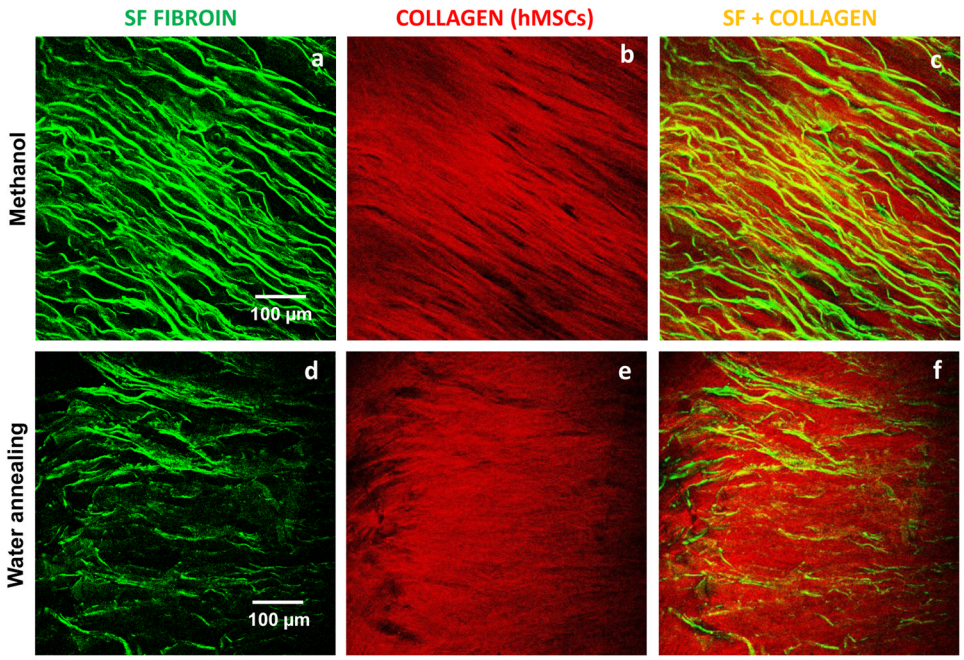

Figure 10.

Multi-photon microscopy evaluation of the lamellar 3D scaffolds treated with methanol and water annealing and after the construct was cultured up to 3 weeks. In green is the two-photon excited fluorescence image of the silk scaffolds (a) treated with methanol and (b) water annealed. In red is the SHG signal from the deposited collagen for the respective treatments (c,d).

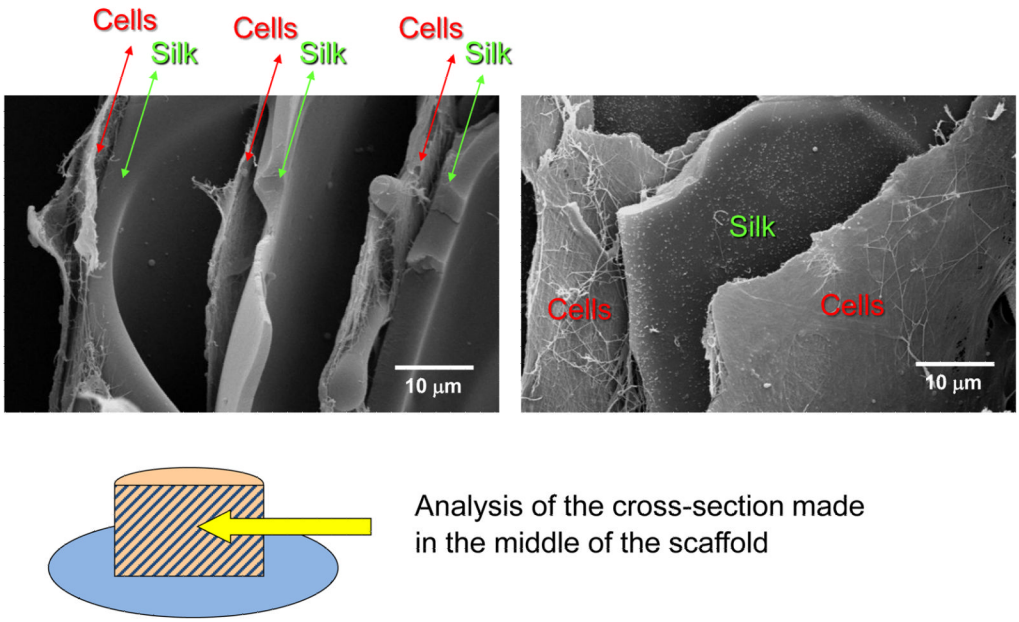

Figure 11.
SEM of a cross-section of a lamellar scaffold treated with methanol, after culture with hMSCs for 3 weeks.

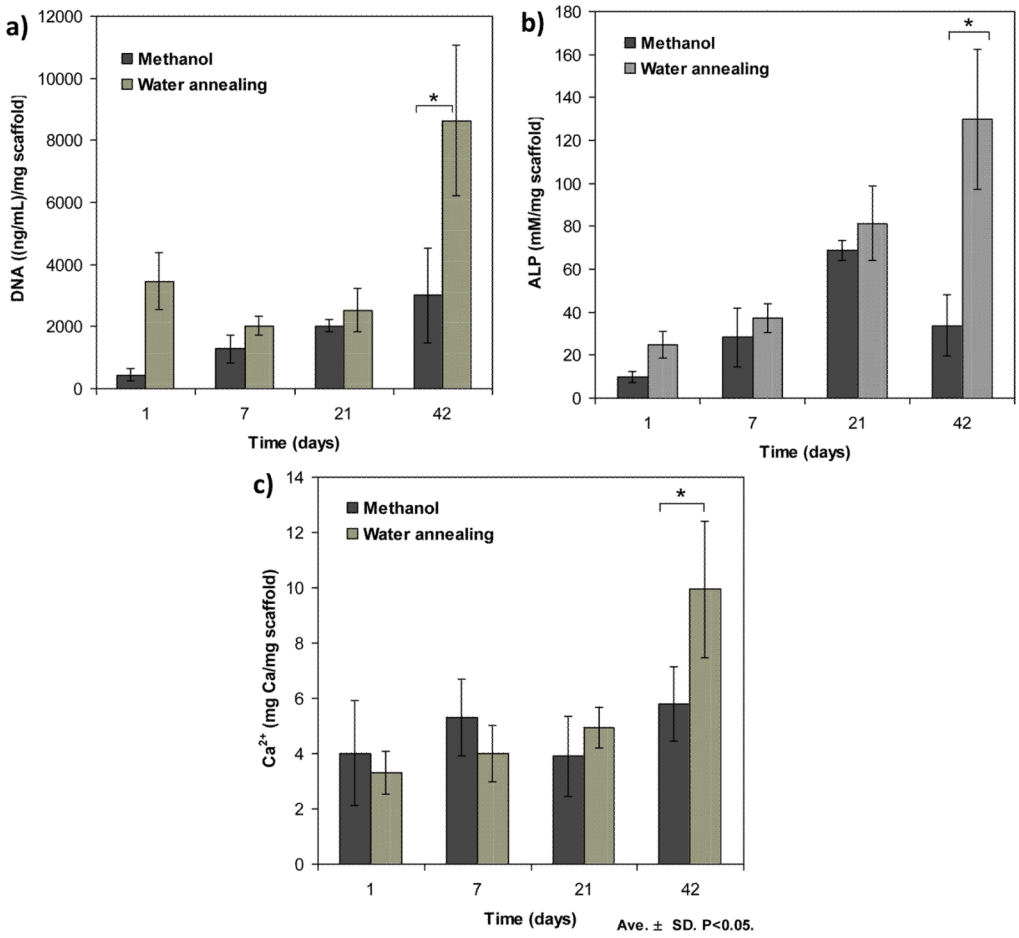

Figure 12.

Biochemical characterization of a) ALP, b) DNA and c) Ca^{2+}, for hMSCs cells cultured up to 6 weeks. Data are shown as mean ± standard deviation from N=4 samples, (*) represents statistically significant differences ($p<0.05$).

Table 1

Vibrational band assignments for the amide I region of silk fibroin [45, 49].

Wavenumber range (cm^{-1})	Secondary structure assignment
1,605–1,615	(Tyr) side chains/aggregated strands
1,616–1,621	Aggregate β-strand/sheet (weak)[a]
1,622–1,627	β-Sheets (strong)[a]
1,628–1,637	β-Sheets (strong)[b]
1,638–1,646	Random coils/extended chains
1,647–1,655	Random coils
1,656–1,662	α-Helix
1,663–1,670	Turns
1,671–1,670	Turns
1,671–1,685	Turns
1,686–1,695	Turns
1,697–1,703	β-Sheets (weak)[a]

[a] Intermolecular β-sheets;

[b] Intramolecular β-sheets

Table 2

Calculated values for the contributions to amide I.

	NC	Water Annealing	Autoclave	Methanol
b-sheet	9,02	23,70	51,26	51,24
Turns	21,50	16,81	18,39	12,87
A-Helix	20,28	15,74	9,79	10,16
R-coil	49,19	42,28	17,98	23,20
S-Chain	0	1,47	2,66	2,52
Silk I	90,97	76,30	48,82	48,75